https://doi.org/10.5194/egusphere-2026-323
Preprint. Discussion started: 29 January 2026

Effect of vertical wind shear on convective clouds: development, organization, and turbulence.

Gaston Bidou[1], Didier Ricard[1], and Christine Lac[1]

[1]CNRM, Université de Toulouse, Météo-France, CNRS, Toulouse, France

Correspondence: Gaston Bidou (gaston.bidou@meteo.fr) and Didier Ricard (ricard.didier@meteo.fr)

Abstract.

This study investigates the influence of vertical wind shear (hereafter "shear") on deep convective clouds. Using a set of high-resolution Large-Eddy Simulations (LES) produced with the research model Meso-NH and spanning a range of shear intensities, we analyse how variations in shear affect storm organisation and intensity. As shear increases, storms exhibit stronger precipitation, more vigorous updrafts, and more intense cold pools beneath the convective cells. When the shear becomes sufficiently strong, the convective cells evolve into supercells, drastically changing the storm regime and highlighting a non-linearity in the behaviour of convective systems. Turbulent quantities are also affected, with higher subgrid and resolved turbulent kinetic energy (TKE) for stronger storms. Moreover, upwind TKE exceeds downwind TKE, although the ratio of subgrid to total TKE remains unchanged across simulations. Using four different organisation metrics, a robust increase in convective organisation is diagnosed with increasing shear, with the supercell regime diverging from the other simulations. Vertical wind shear, through its effect on convective organisation, significantly modifies the characteristics of deep convective storms, and should therefore be taken into account in convective parametrisation schemes.

1 Introduction

Convective storms are a major source of high-impact precipitation events (Doswell, 2001), and their frequency is expected to increase under anthropogenic climate change (Tippett et al., 2015; Prein et al., 2017; Peleg et al., 2025). Accurately forecasting convective storms and the associated phenomena remains challenging, not only because of the variety and complexity of elements, such as hail (Lac, 2014) and lightning strikes (Goodman and MacGorman, 1986; Mazur and Rust, 1983), but also because convective systems are highly sensitive to their environment (Kirkpatrick et al., 2007).

It is well established that vertical wind shear plays a crucial role in organising deep convection. From the pioneering numerical simulations of Weisman and Klemp, 1982 (hereafter WK82) to the Thompson et al., 2007 data reanalysis and the modelling study of Coffer and Parker, 2015, all studies agree on this. However, its influence on convection initiation, and its more subtle effects during the developing and mature phases still require quantitative assessment.

During the initiation phase, several mechanisms have been proposed. On one hand, wind shear bends thermals, reducing vertical velocities (Peters et al., 2019) and potentially inhibiting convection initiation. On the other, bending the thermals may

https://doi.org/10.5194/egusphere-2026-323
Preprint. Discussion started: 29 January 2026

help trigger and organise deep convection. Helfer et al., 2020 shows that both mechanisms operate : shear delays the rise of hot air via thermals and weakens wind velocities, yet remains a necessary condition for sustained deep convection.

During the developing and mature phases, low-level wind shear strongly influences storm motion (Klemp and Wilhelmson, 1978; Rotunno and Klemp, 1982; Weisman and Klemp, 1984; Peters et al., 2020). Several hypotheses have been proposed to explain how shear organises deep convection.

Bending of thermals horizontally may separate the heat source and the updraft core from precipitation resulting from the convection of moist air, preventing cooling of both the heat source and the updraft. Helfer et al., 2020 and Helfer and Nuijens, 2021 compared simulations with and without shear, as well as under "backward shear" conditions, and confirmed that without proper vertical wind shear, precipitation falls into or upwind of the updraft, leading to weaker convective fluxes.

Another hypothesis is that bending of thermals broaden the updraft, reducing the dissipating effect of the entrainment of cold, dry air into the updraft. Entrainment itself is strongly modified under shear : thermals under strong shear conditions entrain environmental air in peculiar ways (LeBel and Markowski, 2023), and convective systems under shear entrain more than their non-sheared counterparts.

Helfer and Nuijens (2021) further showed that overly strong shear can inhibit the development of secondary convective updrafts triggered from cold pools. This “successive feeding” mechanism, whereby new convective cells develop from the remnants of previous ones was studied by Misumi et al., 1994. One notable consequence is the systematic upwind tilting of subsequent convective structures.

In this study, we investigate how vertical wind shear influence both the initiation and development of deep convective clouds using a set of high-resolution Large-Eddy Simulations (LES) produced with the research model Meso-NH with varying shear. Emerging relationships between shear magnitude and the organisation and intensity of the convective systems are examined.

Section 2 describes the model configuration and dataset. Section 3 presents the diagnostics performed, and the trends they unveil. Those are grouped by themes, first on the characteristics of convection, then on turbulent kinetic energy (TKE), and finally on cold pools and organisation. Section 4 summarises and discusses the results.

2 Methodology

2.1 Model

The simulations are performed with the Meso-NH model (Lac et al., 2018), initially developed by CNRM and the Laboratoire d’Aérologie as a research model for simulating atmospheric phenomena from the meso-scale to the microscale. It solves the anelastic formulation of the pseudo-incompressible system of Durran (1989) to filter acoustic waves. Spatial discretisation relies on the Arakawa C-grid. Time integration used in this study is the explicit 4th-order centered Runge-Kutta (RKC4) associated with a 4th-order centered advection scheme. The microphysics scheme is the one-moment ICE3 scheme (Pinty and Jabouille, 1998). It represents 5 prognostic hydrometeors (cloud water, cloud ice, rain, snow, and graupel). Turbulence is parameterised using a 1.5-order closure (Cuxart et al., 2000), i.e. with a prognostic equation for TKE. In LES mode, turbulence is 3D, taking into account horizontal turbulent fluxes, and the mixing length is determined by the mesh size and stability criteria

https://doi.org/10.5194/egusphere-2026-323
Preprint. Discussion started: 29 January 2026

following Deardorff (1980). No shallow convection scheme is used since convective structures are explicitly resolved at LES resolution.

Radiative processes are omitted in order to isolate shear effects. This also contributes to reduce computational and environmental costs (Appendix C). As a result, the domain experiences a gradual increase in total energy because surface heating is included but radiative cooling is not. As such, it limits the total simulation time before becoming unrealistic.

2.2 Data

We have carried out large eddy simulations of deep convection in idealised situations. The domain is an 80-kilometre square with cyclic lateral boundary conditions. Following Strauss et al. (2019), the grid spacing is 50 m in the horizontal. The vertical resolution is 50 m up to 13 km above ground level (AGL) then a smooth stretching is applied until 20 km, yielding a total of 292 vertical levels. The time step ranges from 1 to 0.75 s, depending on maximum wind speed, to satisfy the CFL condition. Each simulation is run for 6 hours.

Initial thermodynamic profiles are taken from the analytical vertical profiles of WK82, with a constant mixing ratio of water vapour in the boundary layer (0.012 kg/kg). Surface fluxes are prescribed, constant and spatially uniform, with 200 $\mathrm{W/m^2}$ for sensible heat and 350 $\mathrm{W/m^2}$ for latent heat.

Convection is triggered using a white-noise perturbation in potential temperature of amplitude 0.2 K within the lowest 1 km. This ensures the loss of stability required to initiate convective motion. Another way of initiating convection would be to introduce a warm bubble near the surface, as done by Verrelle et al., 2015 and LeBel and Markowski, 2023, however we fear this may introduce a characteristic size for convective systems, and avoided this method.

Ten simulations were performed, detailed in table 1, differing only in their initial wind speed profiles. Wind shear was prescribed using quarter-circle hodographs with different horizontal wind magnitudes, from 0 to 20 $\mathrm{m.s^{-1}}$, and shear-layer depths, from 0-1 km to 0-3 km (Figure 1 a). The combination of those two parameters was summarised into a single metric to characterise each simulation : the 0-6 km mean wind shear as a proxy for the bulk Richardson number, since the initial CAPE is constant across experiments. Note that one simulation (W0_S0) is run without wind, and another (W10_S0) without shear, with a 10 $m.s^{-1}$ wind, considered as an advection of shear-free environment.

https://doi.org/10.5194/egusphere-2026-323
Preprint. Discussion started: 29 January 2026

Simulation	Wind speed ($m.s^{-1}$)	Mean shear ($m.s^{-1}.km^{-1}$)
W0_S0	0	0
W10_S0	10	0
W5_S34	5	3.4
W7_S49	7	4.9
W10_S63	10	6.3
W10_S70	10	7.0
W10_S72	10	7.2
W12_S86	12	8.6
W15_S106	15	10.6
W20_S144	20	14.4

Table 1. Wind speed and shear per simulation

No forcing is imposed to the wind speed, meaning that the environmental wind is free to evolve during the simulation. This causes an evolution of the mean shear over time, as the kinetic energy feeding the storms is progressively depleted (Figure 1 c). Indeed, the mean shear decreases in all sheared simulations. In contrast, the mean shear in the "advection" simulation W10_S0 increases with time due to surface friction reducing wind speed in the lowest vertical levels.

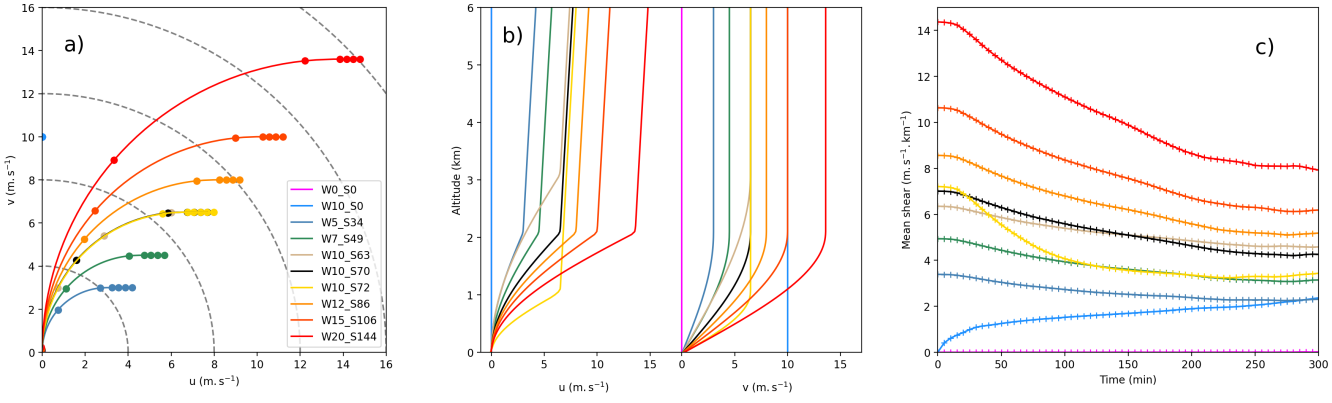

Figure 1. a) Hodographs at the initial conditions, b) horizontal wind components at the initial conditions and c) evolution of mean shear over time for all simulations.

3 Results

In this section, we identify the key differences between the simulations and analyse how various diagnostics respond to changes in mean shear.

https://doi.org/10.5194/egusphere-2026-323
Preprint. Discussion started: 29 January 2026

3.1 Characteristics of the simulated deep convection

Convective structures develop in all simulations. After 5 hours, cumulonimbus clouds reaching up to 12 km AGL are present. This is confirmed by vertical cross sections of clouds, such as the one in Figure 2. It is extracted from the reference simulation at 300 minutes (see dashed line in Figure 3), and shows a deep convective cloud, extending from 2 to 12 km AGL. A convective core is clearly present, with updraft velocities reaching 30 $\mathrm{m.s}^{-1}$, and compensating subsidence in the anvil and around the ascending core. Non-precipitating hydrometeor contents confirm that it is a mixed-phase cloud composed of both liquid water and ice. Note that the liquid part extends higher within the updraft, likely due to temperature anomalies or to supercooled water. Precipitating hydrometeors are also present: rain within and below the updraft, and snow and graupel at higher levels. Graupel mixing ratios are substantial, as expected from the ICE3 microphysics scheme (Lascaux et al., 2006).

Overall, the simulated structures are consistent with LES of deep convective clouds, with explicit circulation within the clouds and well-defined cumuliform structures. This validates our approach and motivates further analysis.

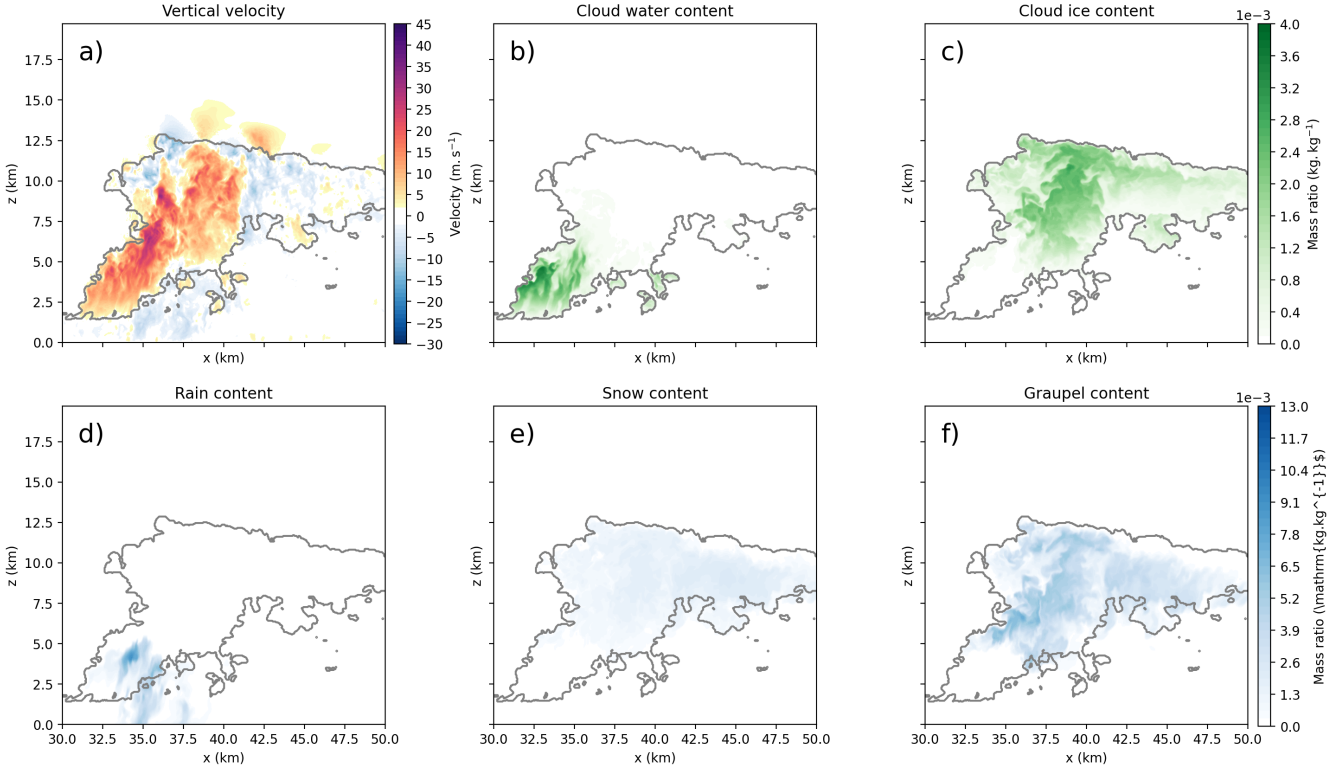

Figure 2. Vertical cross sections for simulation W10_S70 at 300 minutes. a) Vertical velocity and hydrometeor mixing ratios : b) cloud water, c) cloud ice, d) rain, e) snow and f) graupel.

We first examine the simulations by computing the column-averaged vertical velocity over the domain (Figure 3). To highlight the correlation with the cloud cover, we overlay the cloud contour in grey. A grid point is classified as cloudy when

https://doi.org/10.5194/egusphere-2026-323
Preprint. Discussion started: 29 January 2026

the mixing ratio of cloud hydrometeors (the sum of cloud water and cloud ice) exceeds 1.10^{-6} kg/kg. The cloud contour corresponds to the horizontal projection of the total cloud mask (Appendix A).

From these diagnostics, we notice that weakly sheared simulations develop convective cores with smaller area and weaker updrafts. However, no systematic intensification can be seen when comparing the most strongly sheared simulations to intermediate ones.

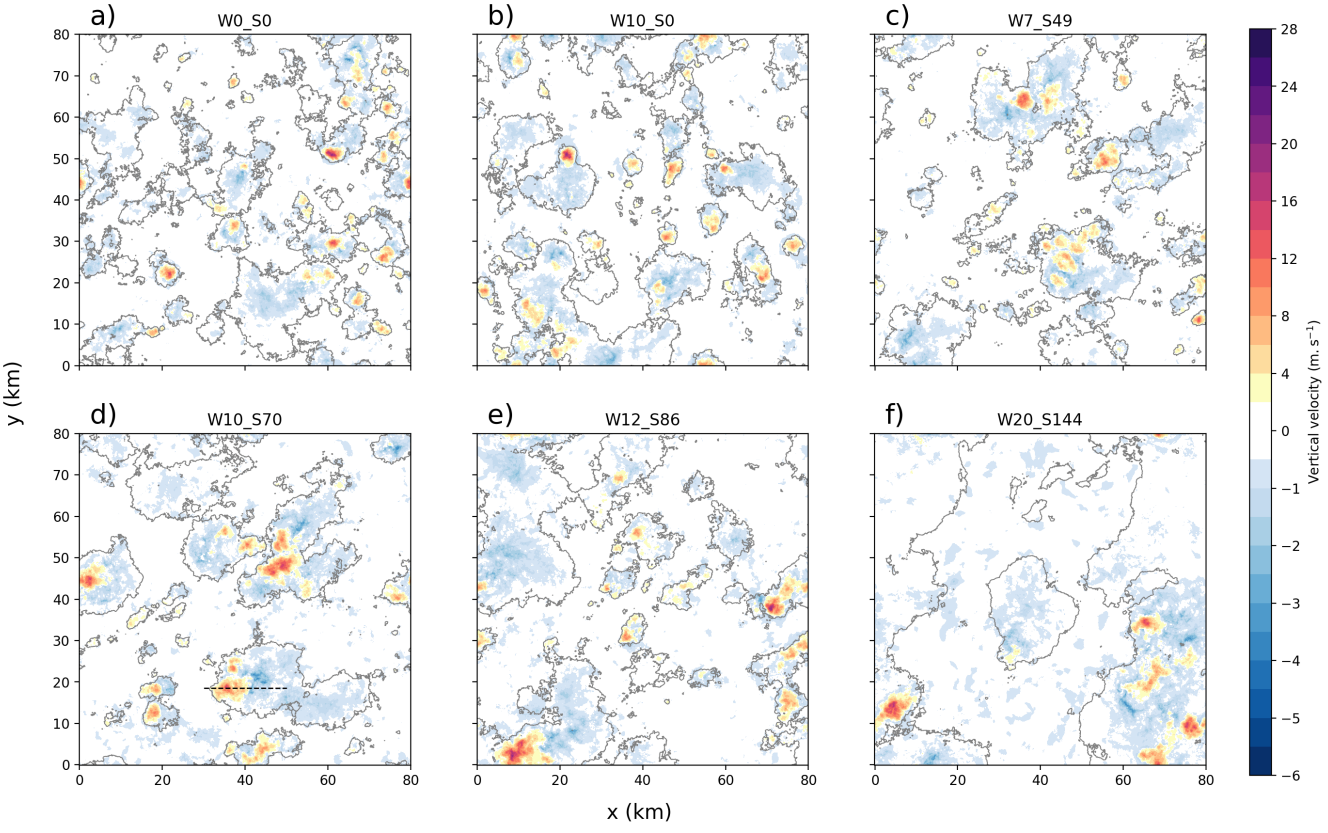

Figure 3. Column-averaged vertical velocity for several simulations at 300 minutes. Grey contour represents clouds. a) - f) correspond to different simulations.

To track the evolution of core intensity, we compute the mean vertical velocity in updraft cores over the whole domain at each output time (every 5 minutes). Figure 4 a shows that mean updraft velocity increases over time (up to 300 minutes) for all simulations except the two with the strongest shear. In those cases, the mean updraft velocity peaks around 200 minutes before decreasing. Updraft helicity (Figure 4 b) computed within the convective cores (Kain et al., 2008) shows the same behaviour, with the largest contrast between the two most strongly sheared simulations and the others occurring around 200 minutes. From this, we isolate two study periods : 150-210 minutes and 240-300 minutes. The first one during the growth phase captures the energy maximum in the two most strongly sheared simulations, while the second one represents the final hour of convective development in the other simulations.

https://doi.org/10.5194/egusphere-2026-323
Preprint. Discussion started: 29 January 2026

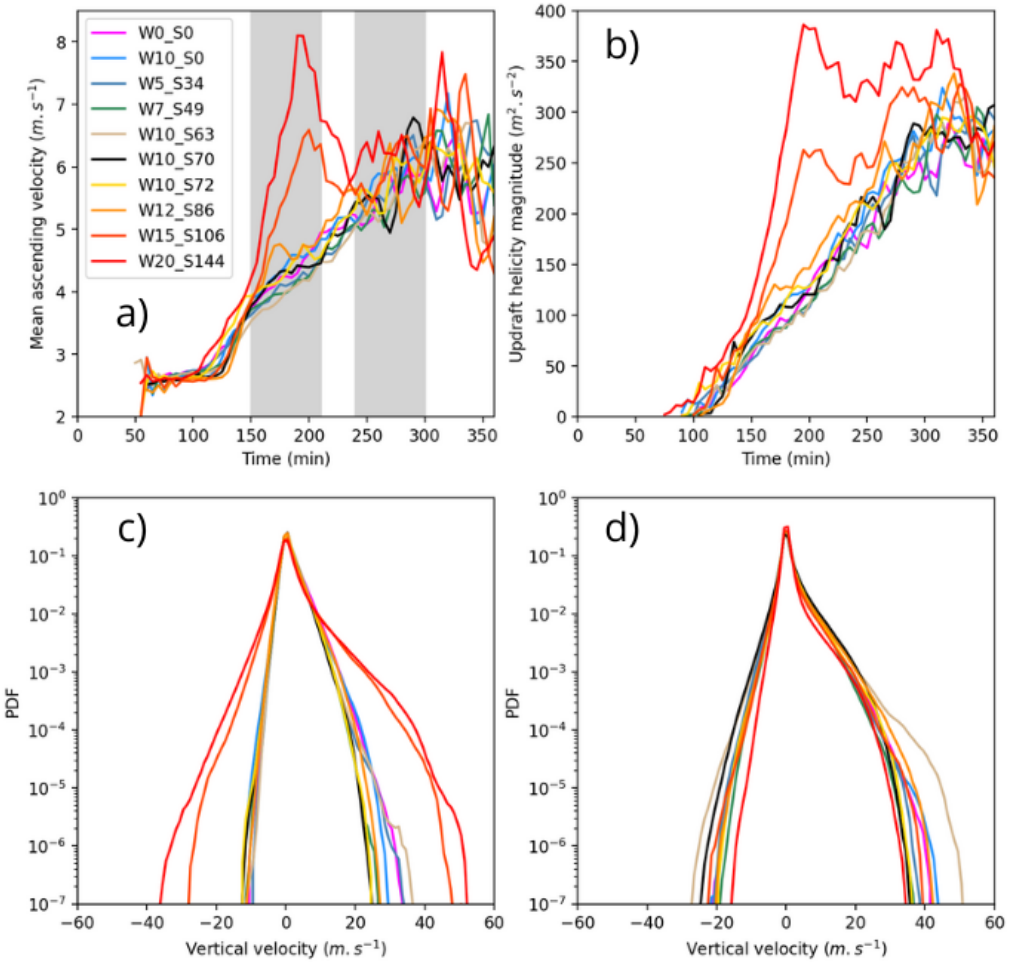

Figure 4. a) Evolution of ascending vertical velocity in updraft cores. b) Evolution of magnitude of updraft helicity in updraft cores. Distribution of vertical velocities in clouds, a) 150-210 minutes and b) 240-300 minutes.

For each of these two periods, we compute the distribution of vertical velocities inside clouds for all simulations (Figure 4 c and d). Between 150 and 210 minutes, the two most strongly sheared simulations show distributions with markedly larger extrema, whereas between 240 and 300 minutes, the other simulations have caught up, while those two show diminished values.

To gain further insight, Figure 5 displays the column-averaged vertical velocity for simulation W20_S144 at 180, 190 and 200 minutes. A storm-splitting process occurs, producing a few large updraft cores with very strong vertical velocities. The same behaviour is observed in simulation W15_S106. These supercells correspond to the maxima shown in Figure 4 a, which persist only briefly before dissipating. This is confirmed in Figure 3: at 300 minutes, the two most strongly sheared simulations no longer exhibit the large updraft cores present at 200 minutes, indicating that the convective systems have largely weakened by that time.

https://doi.org/10.5194/egusphere-2026-323
Preprint. Discussion started: 29 January 2026

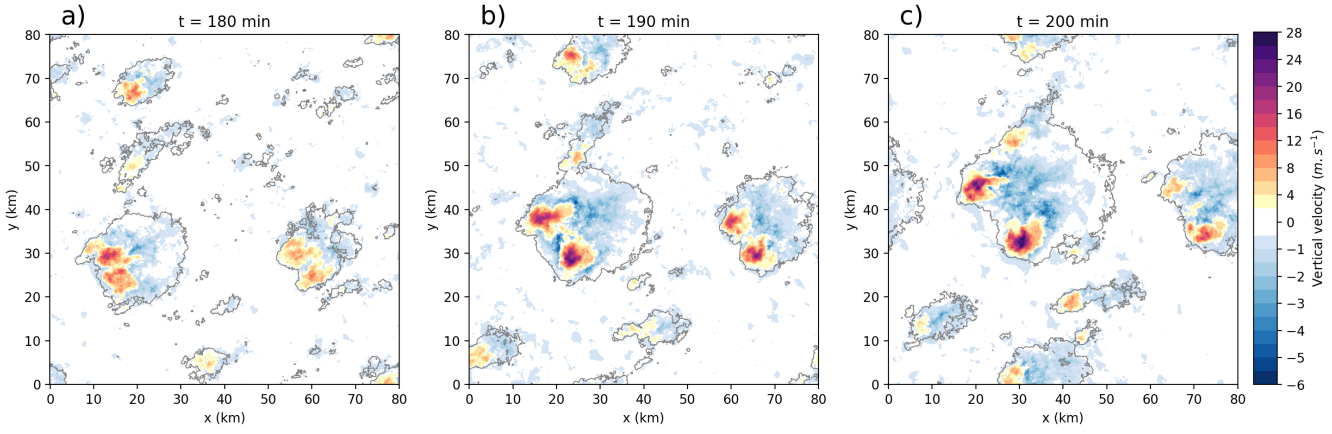

Figure 5. Column-averaged vertical velocity for simulation W20_S144 at different times. Grey contours represent clouds. Left to right : 180 minutes, 190 minutes and 200 minutes.

Differences in storm regimes influence several associated phenomena. Regarding precipitation, we compute the domain-averaged accumulated precipitation. Its evolution reveals a robust trend of increasing precipitation with increasing wind shear (Figure 6 a), with a significant difference between the two most strongly sheared simulations and the others. After 6 hours, the supercell-producing simulations result in precipitation totals up to three times greater than the weakly-sheared ones. Correlating cloud volume with accumulated precipitation shows an excellent linear relationship across simulations at different time steps, although the slope varies with time. Because such correlations are often performed using cloud area and precipitation (Richards and Arkin, 1981), we also verified that cloud area and cloud volume are themselves well correlated (not shown).

Figure 6 c and d also presents the probability density functions (PDFs) of precipitation at 210 and 300 minutes for all simulations. At 210 minutes, both supercell-inducing simulations show much higher local precipitation amounts than all others. The windless case stands out from the weakly-sheared simulations, exhibiting locally heavier precipitation. This may result from convection initiation happening without inhibition from the shear and precipitating earlier, and from less mobile convective cells due to the absence of wind advection. By 300 minutes, the highest local precipitation amount is reached by W12_S86, the most strongly sheared simulations that does not produce supercells. The two supercell-producing simulations (W20_S144 and W15_S106) have been overtaken in terms of peak precipitation, although they still produce a larger number of moderately high values (5-15 mm). The advection case W10_S0 stands out from all the others with much lower maximum precipitation, likely due to a more homogeneous spatial distribution.

https://doi.org/10.5194/egusphere-2026-323
Preprint. Discussion started: 29 January 2026

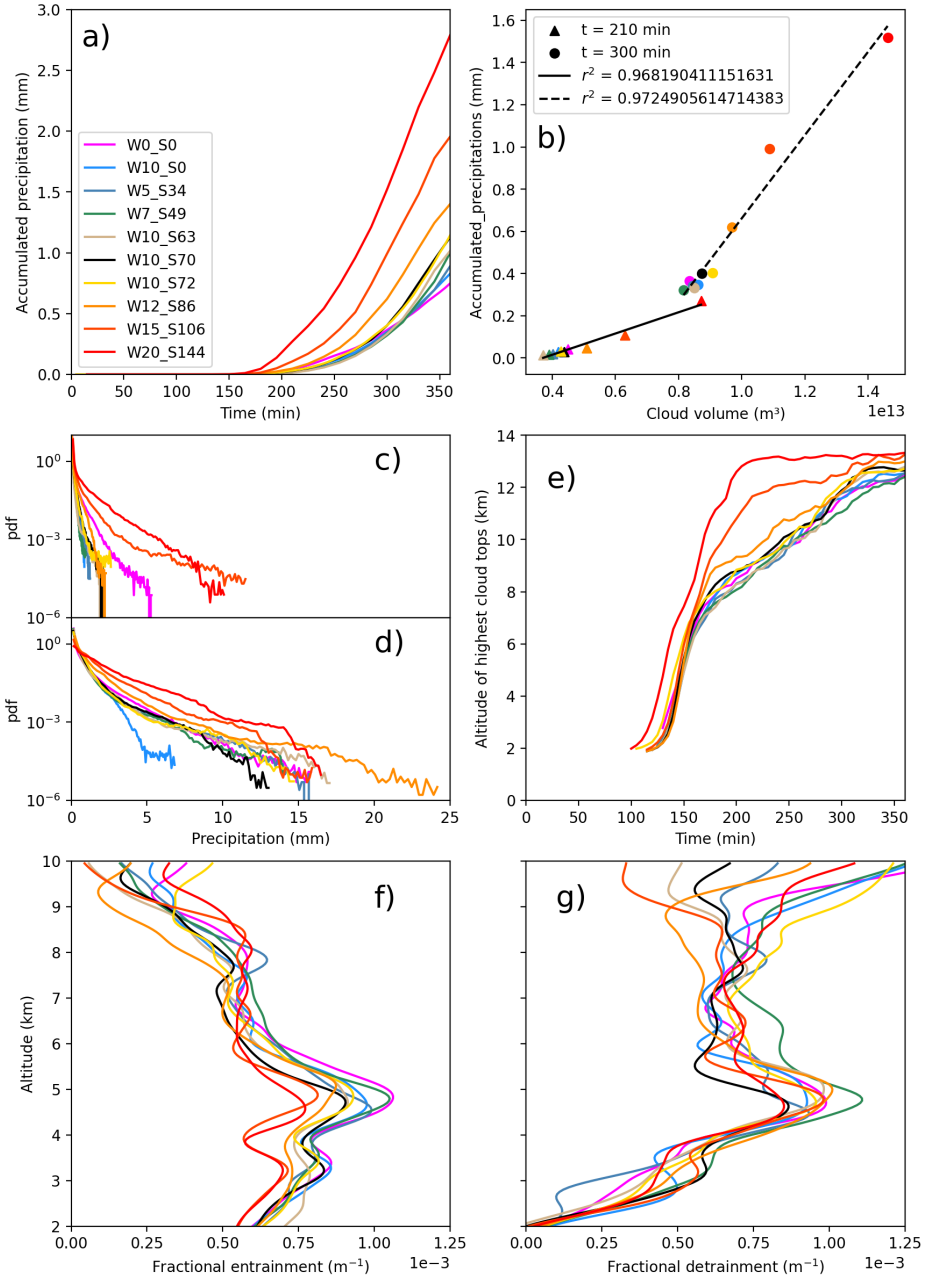

Figure 6. a) Temporal evolution of mean accumulated precipitation. b) Correlation between cloud volume and accumulated precipitation across simulations at 210 and 300 minutes. PDF of accumulated precipitation for all simulations at 210 c) and 300 minutes d). e) Temporal evolution of the highest cloud-top altitude. Vertical profile of f) fractional entrainment and g) fractional detrainment at 300 minutes.

Since supercell-producing simulations develop convection earlier, differences in cloud-top height evolution are expected. To represent the maximum cloud extent more precisely, we compute the mean altitude of the (up to) 100 000 highest cloudy grid

https://doi.org/10.5194/egusphere-2026-323
Preprint. Discussion started: 29 January 2026

points (Figure 6 b). After a quick rise from 2 to 7 km AGL, with similar rates across all simulations, two regimes appear. The two supercell-producing simulations maintain a nearly constant rate of cloud-top ascent until a cap is reached around 12-13 km AGL, imposed by the tropopause. The other simulations show a strong reduction in ascent rate above 7 km, thereafter rising more slowly until reaching a cap around 12 km AGL. No internal differences appear clearly in this second group until reaching the maximum altitude. After 6 hours, all simulations exhibit capped cloud tops, but a trend remains: stronger shear corresponds to higher cloud tops.

However, since the initial CAPE is similar across simulations, the level of neutral buoyancy (LNB) estimated from the initial sounding should be the same in all cases. This difference between the estimated LNB and the simulated cloud-top height can be interpreted as a measure of entrainment dilution (Takahashi and Luo, 2012), as used in previous shear-related studies (Baidu et al., 2022 and Maybee et al., 2024). The reasoning is that the deficit in measured cloud top height stems from an energy loss during the ascent. This is caused by the dilution of cold and dry entrained air into the warm and moist air of the updraft, reducing buoyancy. From this understanding, the higher cloud tops in more strongly sheared environments indicate that their convective cores experience reduced entrainment dilution.

We verified this by computing the entrainment and detrainment at 300 minutes for all simulations (Figure 6 e and f). Using the bulk-plum method for offline computation as described in Siebesma et al. (2003) and Dauhut et al. (2015), we derive fractional entrainment and detrainment profiles. The conservative variable used is the total water mixing ratio. As the computed profiles are very noisy, we used an exponential moving average over the model levels to smoothen the data. The resulting profiles show a trend for more strongly sheared simulations to have lower fractional entrainment, with no trend on the detrainment. This is consistent with the previous hypothesis of shear reducing entrainment dilution of the convective cores.

3.2 TKE

We computed the resolved and subgrid turbulent kinetic energy (TKE) for the simulations. The subgrid TKE is a prognostic variable of the model, whereas the resolved TKE is computed from the velocity components via $e = \frac{1}{2}((\overline{u}-u)^2 + (\overline{v}-v)^2 + (\overline{w}-w)^2)$, with $\overline{u}$, $\overline{v}$ and $\overline{w}$ denoting the wind components averaged over each vertical level. These two values of TKE are then averaged over a time period (240-300 minutes), either on the whole domain or only within clouds. Since the number of cloudy grid points changes with time, the double averaging (over cloud area and over time) requires some care. We chose to represent the average TKE per grid point, normalised by the total number of cloudy points at each vertical level for the full time period. This means that the normalisation differs between vertical levels, but ensures that no cloud point is weighted higher than others due to the temporal variability. Note also that we set the TKE to zero at levels where cloud coverage fell below 3% of the domain, in order to reduce noise near the tropopause and ease interpretation. This does not affect values within the updraft.

Figure 7 shows differences in the resolved TKE in the updraft region (2-8 km AGL). A clear pattern emerges: more strongly sheared simulations exhibit higher resolved TKE, both within clouds and over the full domain. Subgrid TKE remains mostly the same for all simulations. As a result, the ratio of resolved to total TKE increases with shear and consistently exceeds 80%, supporting the classification of these experiments as LES (Pope, 2000). Because TKE is computed here for the 240-300 min

https://doi.org/10.5194/egusphere-2026-323
Preprint. Discussion started: 29 January 2026

time period, the two supercell-inducing simulations are already in a decaying stage, which explains some differences in the curve shapes. TKE values computed over the 150-210 minute time period are higher for these two cases (not shown).

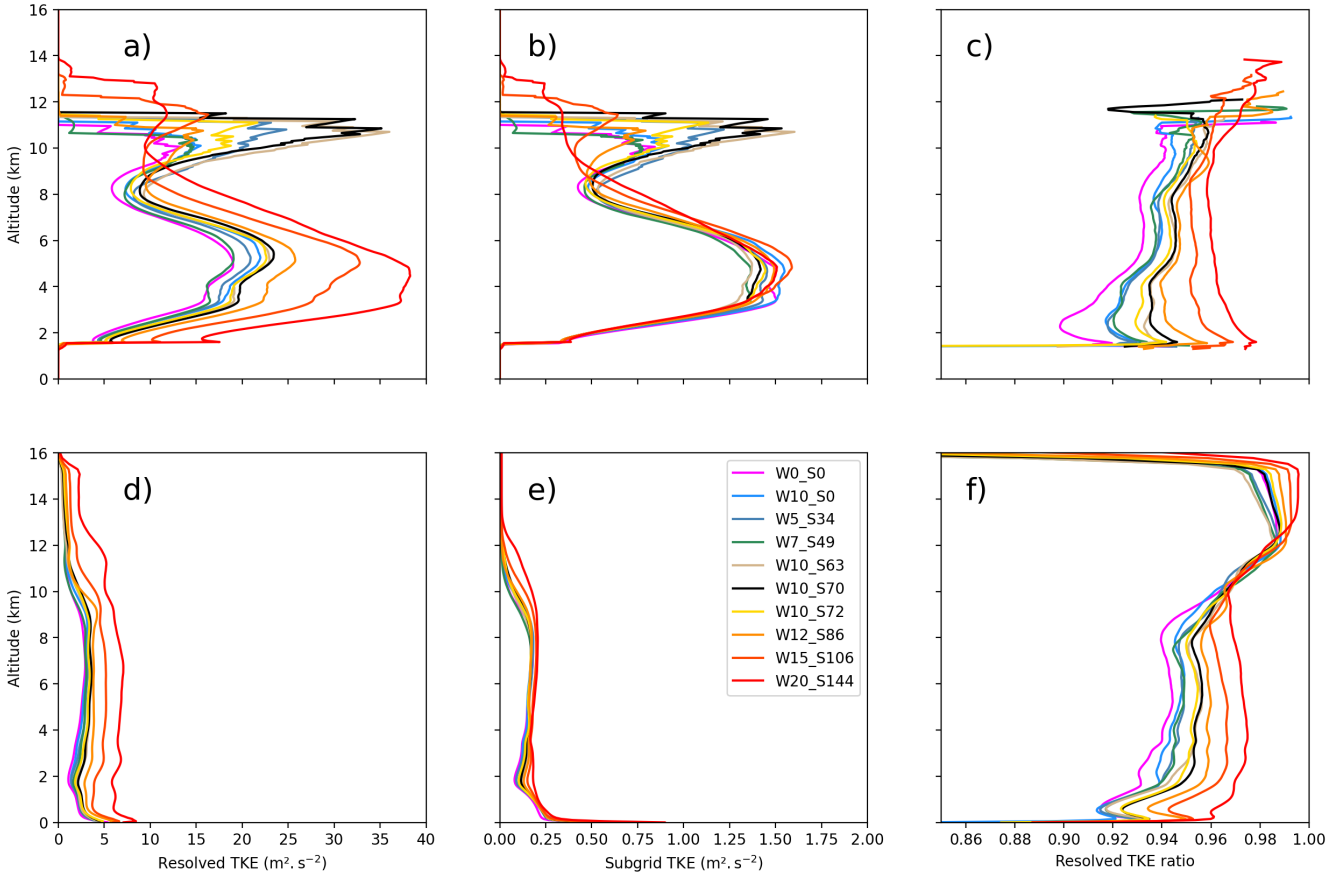

Figure 7. Averaged TKE profiles for all simulations between 240 and 300 minutes. First row within clouds, second row for the whole domain. Columns left to right : resolved TKE, subgrid TKE and ratio resolved/total.

We then investigated how the turbulent quantities would vary between the upwind and downwind regions of the convective cores. Using a dedicated mask that splits the convective cores into separated regions (Appendix B), we computed resolved and subgrid TKE over each mask, with the same normalisation method as above. Here, TKE was set to zero when the convective-core area represented less than 1% of the domain, to reduce noise at high altitude. This choice does not affect updraft values.

In Figure 8, all sheared simulations show systematically higher TKE on the upwind side (dashed lines) compared with the downwind side (solid lines), for both resolved and subgrid TKE, throughout the updraft region (2 - 8 km AGL). The advected case (W10_S0), by contrast, displays almost no difference between upwind and downwind TKE. This is particularly noteworthy, as it suggests that the asymetry depends on the presence of shear rather than on mean advection alone.

https://doi.org/10.5194/egusphere-2026-323
Preprint. Discussion started: 29 January 2026

We also applied this diagnostic to the simulation without mean wind (W0_S0), but do not to show it here, as the definition of upwind and downwind regions hardly applies in that case.

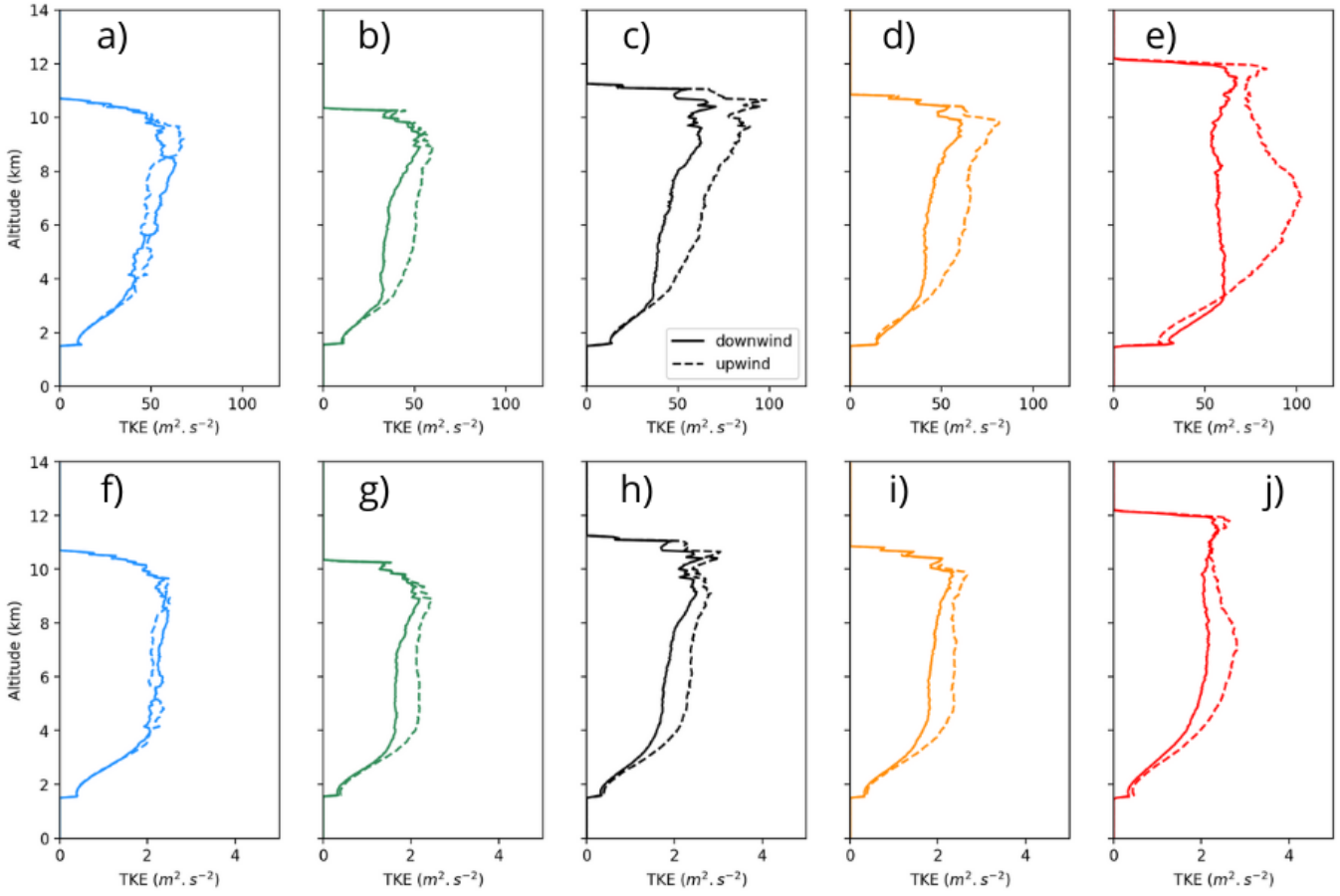

Figure 8. TKE profiles divided between upwind and downwind region for several simulations between 240 and 300 minutes. For simulations W10_S0, W7_S49, W10_S70, W12_S86 and W20_S144, colour coded; a) - e) : resolved TKE; f) - j) : subgrid TKE. Dashed lines upwind, solid lines downwind.

We could expect the difference between upwind and downwind TKE to depend on wind parameters. To compare the magnitude of the asymmetry across simulations, we computed the relative difference $\Delta e_{u,d} = 2\frac{(e_u - e_d)}{(e_u + e_d)}$, for both resolved and subgrid TKE. As shown in Figure 9, no clear relationship can be drawn between shear intensity and the upwind/downwind TKE contrast. The two non-sheared simulations (W0_S0 and W10_S0) show very weak differences, and all the other simulations follow the same patterns, with relative differences reaching up to 0.25 in the updraft region. One possible interpretation is that the TKE asymmetry stems from differences in velocity between the storm and the surrounding flow, with storm motion speed being conditioned by the wind at its base. Shear may cause the environmental wind to exceed the storm motion, which could explain a higher TKE upstream of the convective cores. Another hypothesis, following Lasher-Trapp et al., 2021, would

https://doi.org/10.5194/egusphere-2026-323
Preprint. Discussion started: 29 January 2026

be that an asymmetric "P-shaped" circulation near cloud tops enhances entrainment differently on the upwind and downwind sides, thereby generating the observed TKE contrast.

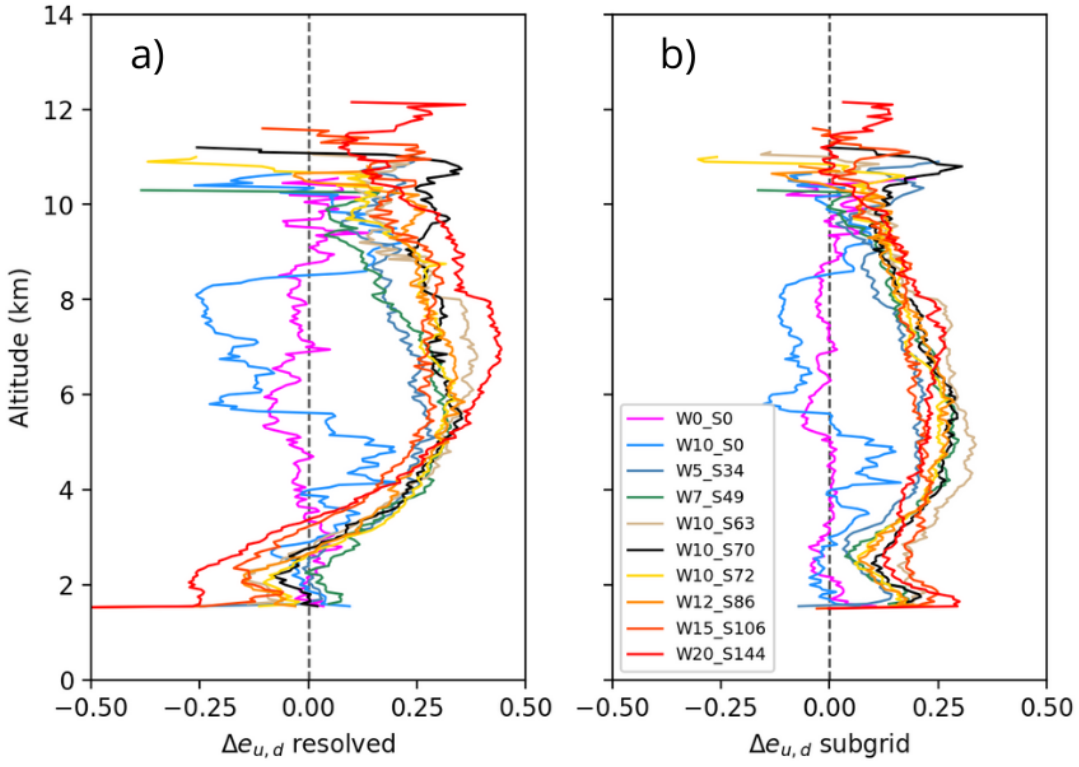

Figure 9. Relative difference between upwind and downwind TKE for all simulations. a) resolved TKE and b) subgrid TKE.

3.3 Cold pools

Convective systems commonly generate cold pools at the surface through the evaporation of raindrops. These cold pools can feed back onto convection initiation, and are therefore of major interest for GCM parametrisation (Rio et al., 2009; Grandpeix and Lafore, 2010). Typically, each convective core produces a single cold pool, and thus variations in convective activity affect cold pool characteristics. To visualise cold pools in the present simulations, we computed the virtual potential temperature θ_v at the first vertical level. Examining the anomaly of θ_v relative to its domain mean reveals the locations of cold pools (Figure 10). At first glance, more strongly sheared simulations produce larger and colder pools, but less numerous. We also note that negative θ_v anomalies are more prominent than positive ones. This motivates a more in-depth statistical analysis.

https://doi.org/10.5194/egusphere-2026-323
Preprint. Discussion started: 29 January 2026

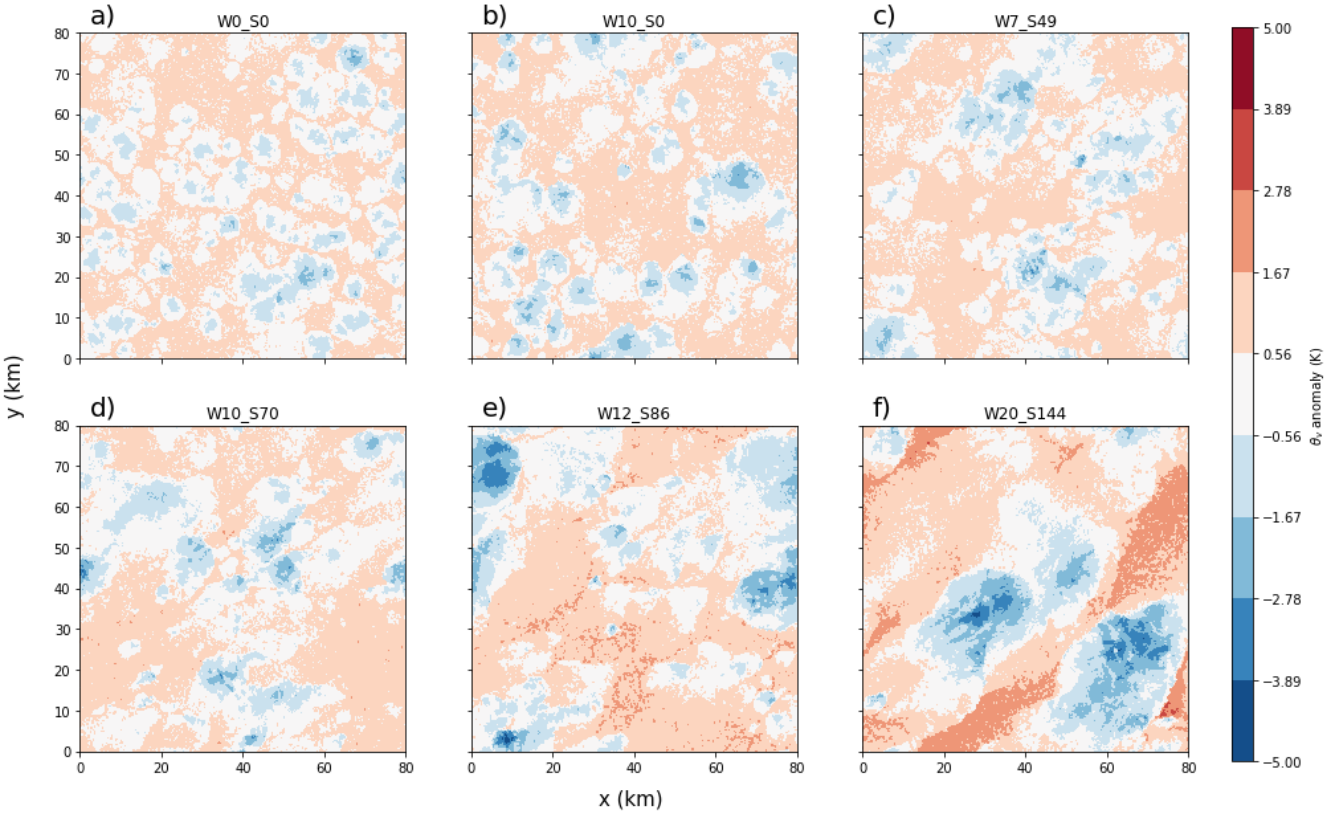

Figure 10. θ_v anomaly for several simulations at 300 minutes. a) - f) correspond to different simulations.

Considering the θ_v anomaly as a distribution, we can examine the evolution of its histogram over time in each simulation. In Figure 11, we observe that for all cases, the temperature at the first vertical level starts to increase (from light to dark colours), due to the surface fluxes. Since these fluxes are maintained throughout the entire simulation, it is important to note that cold-pool formation is dampened by this continuous surface heating, and existing cold pools are progressively eroded. After some time, cold pools begin to appear, and the distribution widens as the temperature decreases locally. Comparing the simulations, we find that the stronger the wind shear, the wider the distribution becomes. Computing the mean and median for each histogram reveals that, in most simulations, the formation of cold pools induces a divergence between these two metrics as the distribution becomes asymmetric. In the most strongly sheared cases, this asymmetry is accompanied by a reduction in the average temperature: surface air cools despite ongoing surface heating.

https://doi.org/10.5194/egusphere-2026-323
Preprint. Discussion started: 29 January 2026

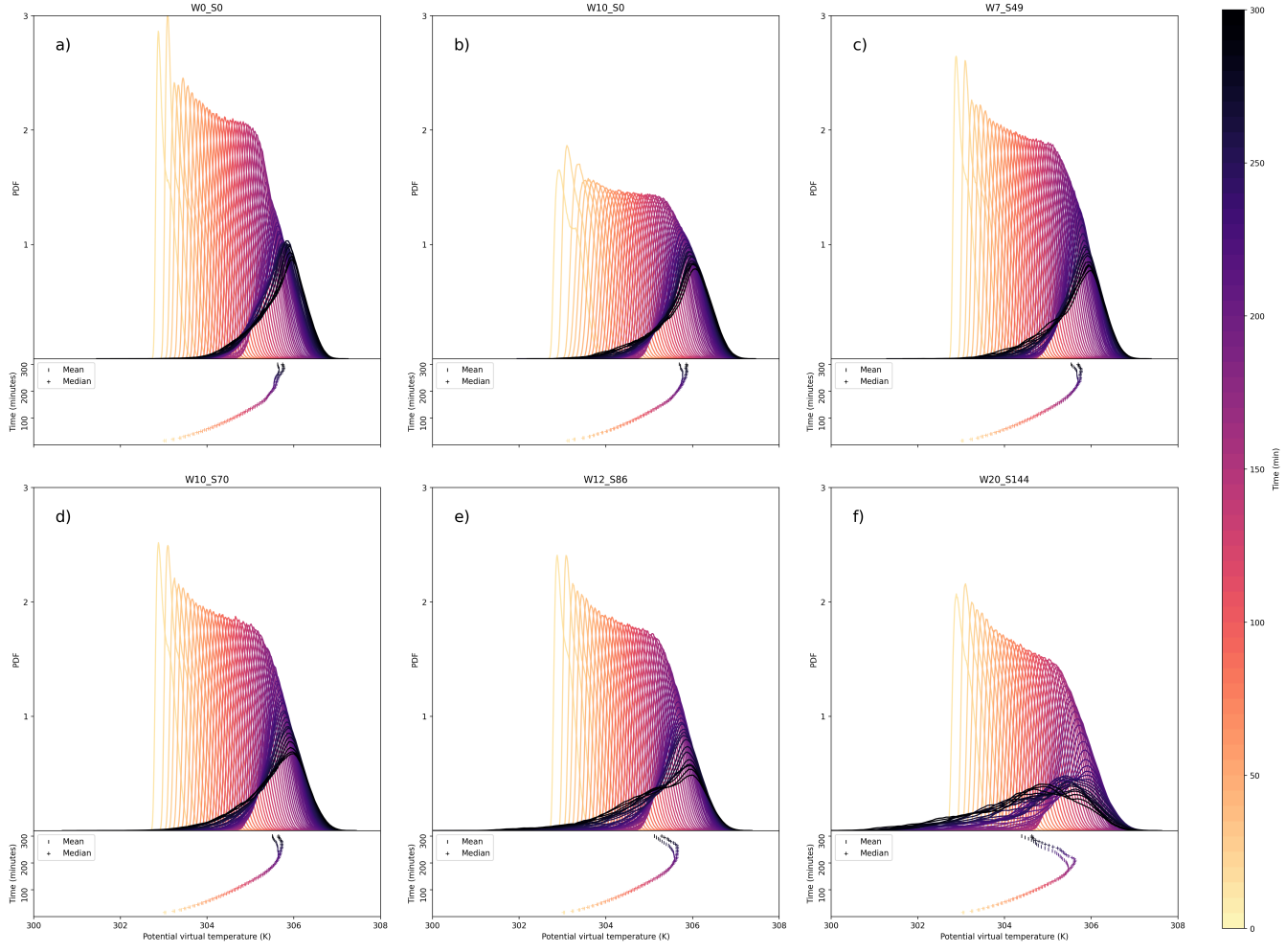

Figure 11. Evolution of θ_v distribution at the first vertical level for several simulations. a) - f) correspond to different simulations.

To better understand this asymmetry, we computed the temporal evolution of several statistical parameters. A side-by-side comparison of means and medians for all the simulations (Figure 12 a and b) emphasises the inclination for more strongly sheared simulations to cool the surface more efficiently. The windless simulation behaves slightly differently from the others. With no wind or shear to inhibit convective initiation, the surface warming slows earlier than in the other simulations due to the first cold pools forming sooner. However, the very low energy convection is insufficient to compensate for the surface heating, and the mean surface temperature caps and stagnates. Regarding the shape of the distribution, the standard deviation (Figure 12 c) increases over time for all simulations, which acts as a proxy for the widening of the temperature distribution. A clear trend emerges: more strongly sheared simulations exhibit larger standard deviation and therefore broader distributions. Finally, examining the skewness of the distribution (Figure 12 d) reveals how the asymmetry evolves. Around the time cold pools begin to form, the distribution shifts from a slight positive skewness to a stronger negative skewness. The initial weak asymmetry is

https://doi.org/10.5194/egusphere-2026-323
Preprint. Discussion started: 29 January 2026

due to random perturbations in the initial conditions, and is quickly overwhelmed by the much stronger asymmetry induced by cold pools around 150 minutes. The two supercell-inducing simulations display the most noteworthy behavior, with a sharp surge in negative skewness coinciding with their energy spike, followed by a gradual decline.

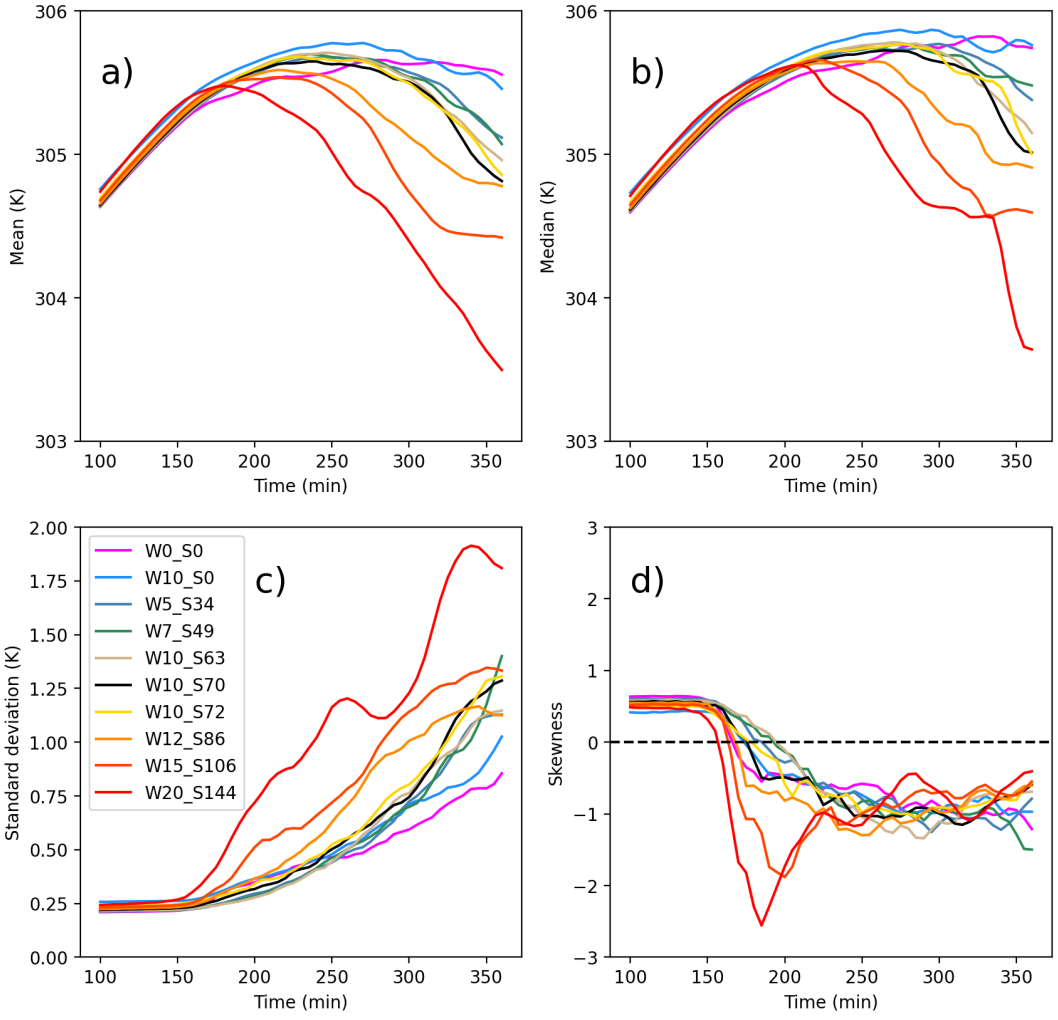

Figure 12. Temporal evolution of statistical parameters of the surface virtual potential temperature θ_v for all simulations. a) - d) : mean, median, standard deviation and skewness.

3.4 Organisation

We hypothesise that many of the differences between our simulations can be related to differences in convective organisation. However, verifying this requires to quantify objectively this organisation. This is challenging, because its definition varies amongst studies (Tobin et al., 2012; White et al., 2018), and no consensus metric has yet emerged. Looking at the convective

https://doi.org/10.5194/egusphere-2026-323
Preprint. Discussion started: 29 January 2026

cores in Figures 5 and 3 suggests a first qualitative trend: more strongly sheared simulations present fewer convective cores, but these cores tend to be larger and more intense. We verified this by computing the number of updraft cores in each simulation (Figure 13 a). Starting from the mask of core points previously defined, we considered any two adjacent core points to belong to the same cluster, accounting for cyclic boundary conditions. This results in numerous core clusters, as isolated core points each form their own cluster. To reduce the influence of the smaller clusters, we computed two different quantities: the total number of core clusters, and the minimum number of cores required to represent 90 percent of the total core volume. The idea is to take into account only the significant core clusters, and to ignore the smallest ones. For this second metric, we observe a clear decrease in the number of updraft cores as shear increases (Figure 13 b), confirming the initial impression that more strongly sheared simulations contain fewer updraft cores.

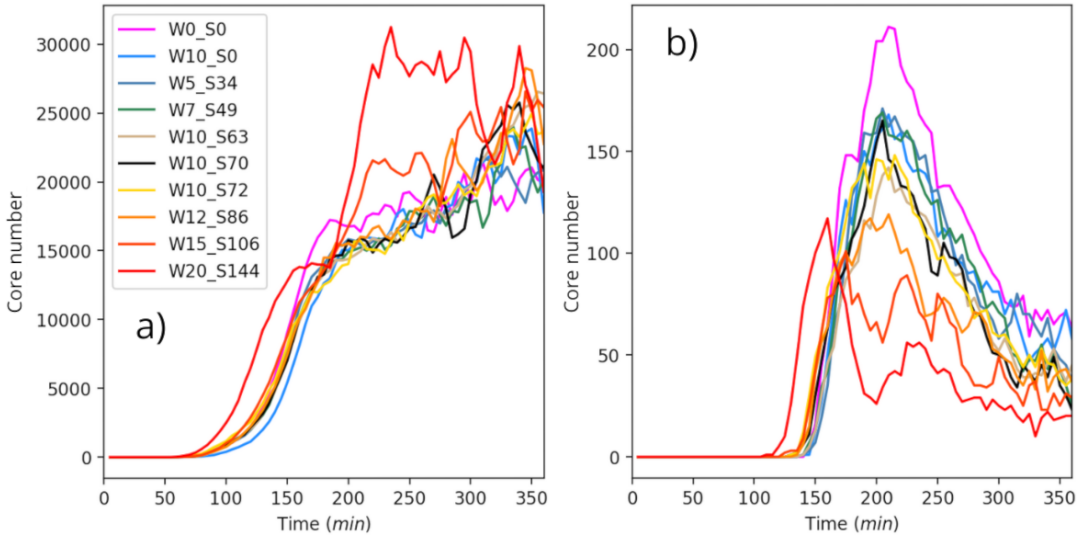

Figure 13. Temporal evolution of updraft core number for each simulation. a) total core number and b) minimum number of cores required to cover 90% of the total core volume at 300 minutes.

Although no single indicator of organisation has yet been isolated, several studies have attempted to narrow down the set of relevant metrics. Janssens et al., 2021 examined 21 different quantities previously used in the literature and applied a statistical reduction method to identify the four indicators that best represent the full set. Their method was applied to satellite images of shallow convection, which differs markedly from our three-dimensional LES data. To address this limitation, we derived 2D cloud masks from our 3D fields, and applied the four selected indicators from Janssens et al. (2021) to our simulations (Figure 14). It is important to note that after 300 minutes, cloud cover has expanded across nearly the entire domain, erasing any meaningful differences between the simulations. Consequently, our analysis focuses on the 150-300 minute period.

https://doi.org/10.5194/egusphere-2026-323
Preprint. Discussion started: 29 January 2026

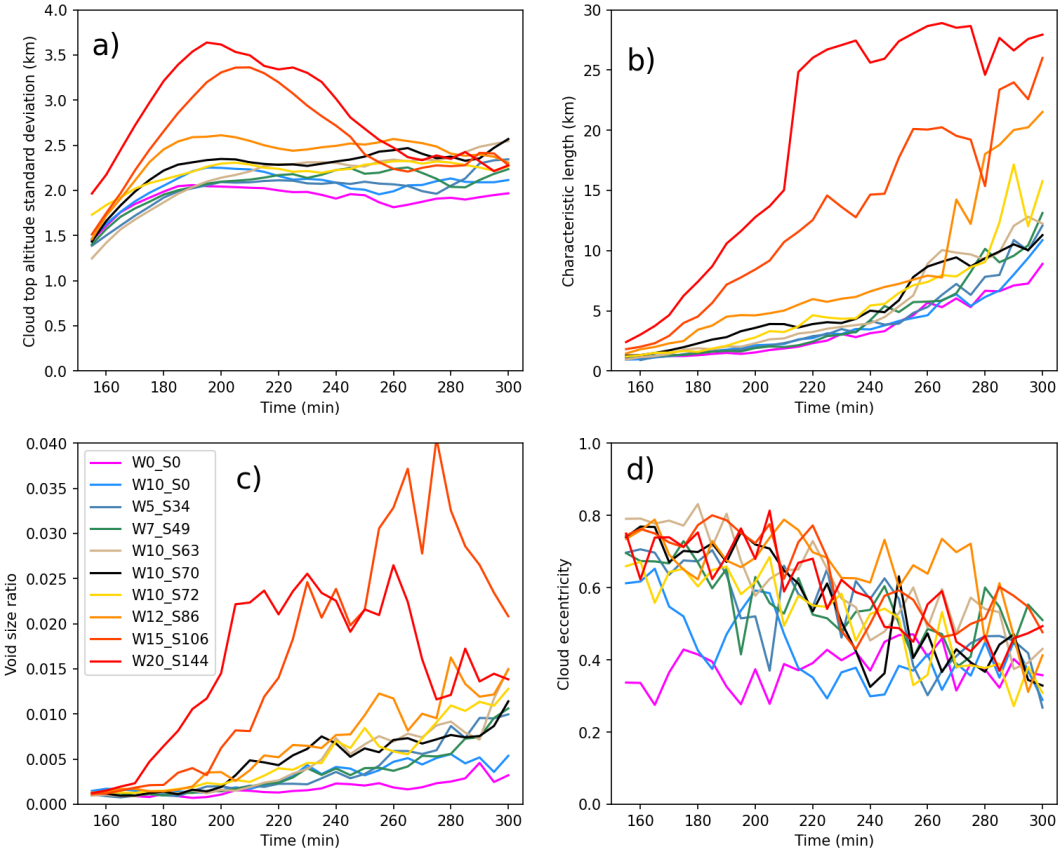

Figure 14. Temporal evolution of 4 characteristic indicators for all simulations. a) - d) : cloud-top height standard deviation, cloud characteristic length, void-size ratio and cloud eccentricity.

Tendencies appear on these graphs. The two most strongly sheared simulations clearly differ from the others across all indicators except eccentricity, exhibiting sharp peaks around their energy maximum at 200 minutes. The storm-splitting process, and the resulting supercells, induce strong variations in cloud radius, void sizes, and cloud-top height standard deviation (Figure 14 a - c). Overall, strong wind shear generates supercells whose signatures can be quantified as marked differences in organisation according to these indicators.

Moreover, both the cloud-top height standard deviation and the void-size ratio increase monotonically with mean shear. This confirms our earlier qualitative impression, based on visual inspection and core-count diagnostics, that more strongly sheared simulations develop more organised convection.

https://doi.org/10.5194/egusphere-2026-323
Preprint. Discussion started: 29 January 2026

4 Conclusion and Discussion

In this study, we used LES to investigate the impact of vertical wind shear on deep convective clouds. We conducted a set of simulations spanning a wide range of shear intensities, supplemented by a windless simulation and one with a uniform advective wind. All simulations develop convective storms, but two distinct regimes emerge. In the two most strongly sheared simulations, supercells form through the storm-splitting process, while the other simulations only develop ordinary convective cells. Since supercells arise exclusively in the most strongly sheared cases, this process requires mean wind shear to exceed a threshold of approximately 10 $\mathrm{m.s^{-1}.km^{-1}}$.

Beyond these two different regimes, we highlight several robust trends in the structure and evolution of convective storms. As a general and qualitative principle, stronger shear produces more intense storms. This conclusion can be supported by multiple diagnostics.

- Precipitation increases markedly with shear. After 6 hours, the most strongly sheared simulation produces nearly four times as much domain-averaged precipitation as the least-sheared one. The distribution of precipitation is also affected by wind shear, with the windless and shearless simulations behaving as notable outliers.
- The two regimes are clearly distinguishable in cloud-top height and ascending speed. The cloud tops of supercells increase continuously to their maximum values, whereas the other simulations display two ascending phases with different ascent rates. After 6 hours, more strongly sheared simulations systematically produce higher cloud tops, consistent with reduced entrainment dilution. Early peaks in mean updraft speed also clearly identify the supercell-producing cases.
- Resolved TKE within clouds increases steadily with shear. This is likely linked to stronger vertical velocity and results in a higher resolved turbulence ratio. Upwind TKE is about 25% greater than downwind TKE in sheared simulations, a ratio that remains almost constant across shear intensities. In contrast, the windless and shearless simulations exhibit negligible differences between upwind and downwind regions.
- Cold pools become larger, colder, and less numerous with increasing wind shear. The distribution of surface virtual potential temperature shows decreasing mean and median values, along with increasing standard deviation, as shear strengthens. This reflects more efficient surface cooling by cold pools. The distribution's skewness also reverses sign, with a pronounced negative spike in the supercell-inducing simulations.
- Convective organisation also varies systematically with shear. In agreement with cold pools, convective cores become larger and fewer as shear increases. Three of the four selected organisation indicators show clear trends with shear: the cloud-top height standard deviation, the characteristic length scale, and the void-size ratio all increase with stronger shear.

Our work has mainly focused on different diagnostics of convection rather than deeply analysing the physical mechanisms underlying the effect of shear on deep convective clouds. Recent hypothesis suggest that low-altitude pressure "footprint" may

https://doi.org/10.5194/egusphere-2026-323
Preprint. Discussion started: 29 January 2026

help sustain updrafts (Peters et al., 2022), while other studies have shown that, in the presence of pre-existing cold pools, an increase in shear kinetical energy enhances updraft velocity (Mulholland et al., 2021).

Our study of cold pools was limited to the virtual temperature at the first model level. In-depth analysis of the structure of cold pools could be achieved using object-based methods (Boeing, 2016 and Rochetin et al., 2021), which are used in some parametrisation of convective initiation (Rooney et al., 2022 and Dauhut et al., 2023). Applying these techniques here could improve our understanding of the relative positions of cold pools and updrafts, and help disentangle cause-and-effect relationships.

Future studies will explore the use of a two-moment microphysical scheme, allowing the explicit representation of droplet and ice crystal size distributions, which may influence evaporation and mixing processes at cloud edges. Besides, simulations in this study were conducted without a radiation scheme. Including radiative cooling in future studies will allow us to investigate its influence on cloud-top processes and cloud-development speed. Finally, this study also provided synthetic cloud datasets to develop retrieval algorithms for the CLOUD visible imagers of the upcoming C3IEL mission (Dandini et al., 2022)). This satellite mission will provide high-resolution observations on cloud-top evolution and ascent rates, which in turn will help validate and improve atmospheric models simulating deep convection.

Appendix A: 2D cloud masks

Computing 2-dimensional cloud masks for 3-dimensional data required some considerations. The challenge consists in determining an appropriate condition for each model column to be classified as cloudy. We tried 3 different approaches, with increasing constraints, and compared the results.

The first approach was to be as large as possible: if any point of a column is cloudy, then the column is to be considered cloudy. We then introduced a total thickness condition, as in at least n points of the column needed to be cloudy (we fixed $n = 30$, meaning at least 1500 m of cloud depth). Finally, we added a continuity condition, so that at least n consecutive points of the column needed to be cloudy, still with $n = 30$. Each approach is more restrictive than the previous one, yet all can be argued for.

We tried all 3 masks for the relevant diagnostics, and chose the one which highlighted the best the appearing trends. For all diagnostics except the void-size ratio, we ended up choosing the total and discontinuous thickness condition. For the void-size ratio, the least restrictive mask showed better results, although the discussed observation was present for all 3 masks.

Appendix B: Upwind/Downwind masks

To compute upwind and downwind turbulent quantities, we had to define a 3-dimensional upwind/downwind mask for the convective cores. Several ideas were attempted, we describe here the approach that produced the best results.

Extending the idea of upstream and downstream to a 3-dimensional field would require an analysis of the streamlines, which is non-trivial due to the turbulent nature of the flow. We therefore restricted the method to a 2-dimensional analysis at each

https://doi.org/10.5194/egusphere-2026-323
Preprint. Discussion started: 29 January 2026

vertical level. At a given level, convective cores were isolated using 2D clustering. For each cluster, every point was projected onto the axis defined by the mean horizontal wind direction at that level. We then defined an upwind and downwind part of each cluster by comparing the position of each point relative to the cluster mean.

Repeating this process for each 2D cluster of a vertical level, and for each vertical levels creates a mask over the whole domain with upwind and downwind regions for each convective core, as seen in Figure A1. This mask was used to compute turbulent quantities in the upwind and downwind parts of convective cores.

Appendix C: Simulation cost

Running these simulations comes at a substantial computational cost. Although access to MeteoFrance's Belenos supercomputer enables the production of such high-resolution LESs, we consider it important to be transparent regarding the resources required.

Each simulation ran for about 100 hours on 8000 cores distributed across 100 nodes, corresponding to about 5% of the supercomputer's capacity for this duration. Using the energy consumption data provided by Belenos, we estimated the monetary and environmental cost of the simulations. However, these data present large fluctuations with some unrealistic spikes. We therefore limited our analysis to averaging the reasonable values. The following calculations are therefore very rough estimates and should be treated as such.

The energy consumption amounts to a total just under 100 MWh for all runs, accounting for those that failed (estimated 30 failed or trial runs for 10 successful ones). Considering France's average yearly consumption of 2.2 MWh/person, producing our data required the energy consumed by more than 40 average French people over a year. With the government-regulated price per kWh for individuals in 2024 of 0.25 €/kWh, a first estimate of the monetary cost for our simulations is 25 k€. This could arguably be lower with corporate rates. The carbon footprint of electricity in France is evaluated by the government-owned RTE electricity transport network. Their data for 2023 show a carbon footprint of 32 g$CO2_{eq}$/kWh for produced electricity. Hence, the estimation of 3.2 tons $CO2_{eq}$ emitted as a result of our computations. This could arguably be higher by taking into account the imported electricity from other European countries. A footprint of 3.2 tons represents about 150% of the 2.2 tons $CO2_{eq}$ individual emission targeted by France's High Council for Climate (HCC) by 2050 in order to limit the global warming to 1.5°C. It is noteworthy that 2023 was a record year for low-carbon electricity in France (RTE), and that the French energy mix is one of the least carbonated amongst European countries (Directorate-General for Energy (European Commission), 2024).

https://doi.org/10.5194/egusphere-2026-323
Preprint. Discussion started: 29 January 2026

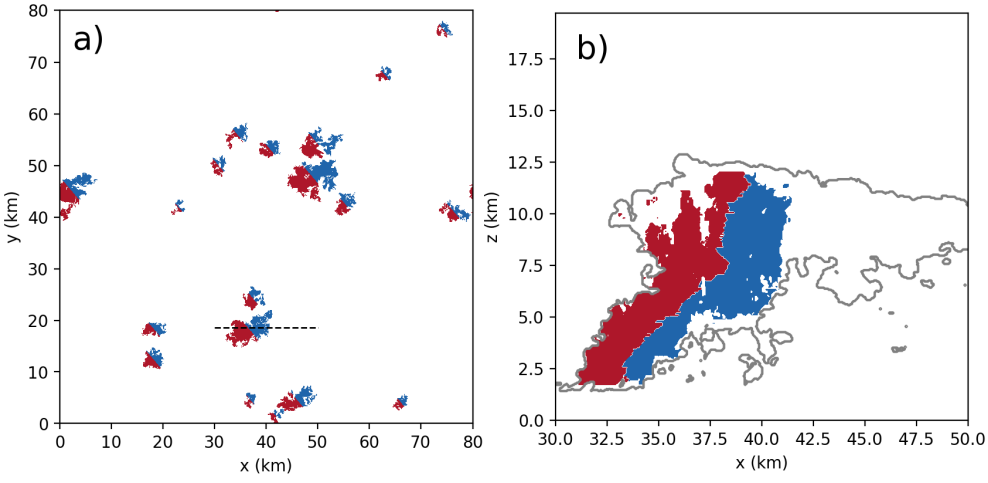

Figure A1. Mask of upwind (red) and downwind (blue) regions of convective cores for simulation W10_S70 at 300 minutes. a) horizontal cross sections at $z = 6$ km and b) vertical slice at $y = 18.5$ km.

https://doi.org/10.5194/egusphere-2026-323
Preprint. Discussion started: 29 January 2026

References

Baidu, M., Schwendike, J., Marsham, J. H., and Bain, C.: Effects of vertical wind shear on intensities of mesoscale convective systems over West and Central Africa, Atmospheric Science Letters, 23, e1094, https://doi.org/10.1002/asl.1094, _eprint: https://onlinelibrary.wiley.com/doi/pdf/10.1002/asl.1094, 2022.

Boeing, S. J.: An object-based model for convective cold pool dynamics, Mathematics of Climate and Weather Forecasting, 2, 43–60, https://doi.org/10.1515/mcwf-2016-0003, number: 1 Publisher: De Gruyter Open, 2016.

Coffer, B. E. and Parker, M. D.: Impacts of Increasing Low-Level Shear on Supercells during the Early Evening Transition, Monthly Weather Review, 143, 1945–1969, https://doi.org/10.1175/MWR-D-14-00328.1, publisher: American Meteorological Society Section: Monthly Weather Review, 2015.

Cuxart, J., Bougeault, P., and Redelsperger, J.-L.: A turbulence scheme allowing for mesoscale and large-eddy simulations, Quarterly Journal of the Royal Meteorological Society, 126, 1–30, https://doi.org/10.1002/qj.49712656202, _eprint: https://rmets.onlinelibrary.wiley.com/doi/pdf/10.1002/qj.49712656202, 2000.

Dandini, P., Cornet, C., Binet, R., Fenouil, L., Holodovsky, V., Y. Schechner, Y., Ricard, D., and Rosenfeld, D.: 3D cloud envelope and cloud development velocity from simulated CLOUD (C3IEL) stereo images, Atmospheric Measurement Techniques, 15, 6221–6242, https://doi.org/10.5194/amt-15-6221-2022, publisher: Copernicus GmbH, 2022.

Dauhut, T., Chaboureau, J.-P., Escobar, J., and Mascart, P.: Large-eddy simulations of Hector the convector making the stratosphere wetter, Atmospheric Science Letters, 16, 135–140, https://doi.org/10.1002/asl2.534, _eprint: https://rmets.onlinelibrary.wiley.com/doi/pdf/10.1002/asl2.534, 2015.

Dauhut, T., Couvreux, F., Bouniol, D., Beucher, F., Volkmer, L., Pörtge, V., Schäfer, M., Ayet, A., Brilouet, P.-E., Jacob, M., and Wirth, M.: Flower trade-wind clouds are shallow mesoscale convective systems, Quarterly Journal of the Royal Meteorological Society, 149, 325–347, https://doi.org/10.1002/qj.4409, _eprint: https://onlinelibrary.wiley.com/doi/pdf/10.1002/qj.4409, 2023.

Deardorff, J. W.: Stratocumulus-capped mixed layers derived from a three-dimensional model, Boundary-Layer Meteorology, 18, 495–527, https://doi.org/10.1007/BF00119502, 1980.

Directorate-General for Energy (European Commission): EU energy in figures: statistical pocketbook 2024, Office des publications de l'Union européenne, ISBN 978-92-68-16603-1, https://data.europa.eu/doi/10.2833/802460, 2024.

Doswell, C. A.: Severe Convective Storms, American Meteorological Society, 2001.

Durran, D. R.: Improving the Anelastic Approximation, Journal of the Atmospheric Sciences, 46, 1453–1461, https://doi.org/10.1175/1520-0469(1989)046<1453:ITAA>2.0.CO;2, publisher: American Meteorological Society Section: Journal of the Atmospheric Sciences, 1989.

Goodman, S. J. and MacGorman, D. R.: Cloud-to-Ground Lightning Activity in Mesoscale Convective Complexes, Monthly Weather Review, 114, 2320–2328, https://doi.org/10.1175/1520-0493(1986)114<2320:CTGLAI>2.0.CO;2, publisher: American Meteorological Society Section: Monthly Weather Review, 1986.

Grandpeix, J.-Y. and Lafore, J.-P.: A Density Current Parameterization Coupled with Emanuel's Convection Scheme. Part I: The Models, Journal of the Atmospheric Sciences, 67, 881–897, https://doi.org/10.1175/2009JAS3044.1, publisher: American Meteorological Society Section: Journal of the Atmospheric Sciences, 2010.

Helfer, K. C. and Nuijens, L.: The Morphology of Simulated Trade-Wind Convection and Cold Pools Under Wind Shear, Journal of Geophysical Research: Atmospheres, 126, e2021JD035 148, https://doi.org/10.1029/2021JD035148, _eprint: https://onlinelibrary.wiley.com/doi/pdf/10.1029/2021JD035148, 2021.

https://doi.org/10.5194/egusphere-2026-323
Preprint. Discussion started: 29 January 2026

Helfer, K. C., Nuijens, L., de Roode, S. R., and Siebesma, A. P.: How Wind Shear Affects Trade-wind Cumulus Convection, Journal of Advances in Modeling Earth Systems, 12, e2020MS002 183, https://doi.org/10.1029/2020MS002183, _eprint: https://onlinelibrary.wiley.com/doi/pdf/10.1029/2020MS002183, 2020.

Janssens, M., Vilà-Guerau de Arellano, J., Scheffer, M., Antonissen, C., Siebesma, A. P., and Glassmeier, F.: Cloud Patterns in the Trades Have Four Interpretable Dimensions, Geophysical Research Letters, 48, e2020GL091 001, https://doi.org/10.1029/2020GL091001, _eprint: https://onlinelibrary.wiley.com/doi/pdf/10.1029/2020GL091001, 2021.

Kain, J. S., Weiss, S. J., Bright, D. R., Baldwin, M. E., Levit, J. J., Carbin, G. W., Schwartz, C. S., Weisman, M. L., Droegemeier, K. K., Weber, D. B., and Thomas, K. W.: Some Practical Considerations Regarding Horizontal Resolution in the First Generation of Operational Convection-Allowing NWP, Weather and Forecasting, 23, 931–952, https://doi.org/10.1175/WAF2007106.1, publisher: American Meteorological Society Section: Weather and Forecasting, 2008.

Kirkpatrick, J. C., McCaul, E. W., and Cohen, C.: The Motion of Simulated Convective Storms as a Function of Basic Environmental Parameters, Monthly Weather Review, 135, 3033–3051, https://doi.org/10.1175/MWR3447.1, publisher: American Meteorological Society Section: Monthly Weather Review, 2007.

Klemp, J. B. and Wilhelmson, R. B.: Simulations of Right- and Left-Moving Storms Produced Through Storm Splitting, Journal of the Atmospheric Sciences, 35, 1097–1110, https://doi.org/10.1175/1520-0469(1978)035<1097:SORALM>2.0.CO;2, publisher: American Meteorological Society Section: Journal of the Atmospheric Sciences, 1978.

Lac, C.: Peut-on prévoir les orages de grêle ?, La Météorologie, pp. 34–37, https://doi.org/10.4267/2042/54334, 2014.

Lac, C., Chaboureau, J.-P., Masson, V., Pinty, J.-P., Tulet, P., Escobar, J., Leriche, M., Barthe, C., Aouizerats, B., Augros, C., Aumond, P., Auguste, F., Bechtold, P., Berthet, S., Bielli, S., Bosseur, F., Caumont, O., Cohard, J.-M., Colin, J., Couvreux, F., Cuxart, J., Delautier, G., Dauhut, T., Ducrocq, V., Filippi, J.-B., Gazen, D., Geoffroy, O., Gheusi, F., Honnert, R., Lafore, J.-P., Lebeaupin Brossier, C., Libois, Q., Lunet, T., Mari, C., Maric, T., Mascart, P., Mogé, M., Molinié, G., Nuissier, O., Pantillon, F., Peyrillé, P., Pergaud, J., Perraud, E., Pianezze, J., Redelsperger, J.-L., Ricard, D., Richard, E., Riette, S., Rodier, Q., Schoetter, R., Seyfried, L., Stein, J., Suhre, K., Taufour, M., Thouron, O., Turner, S., Verrelle, A., Vié, B., Visentin, F., Vionnet, V., and Wautelet, P.: Overview of the Meso-NH model version 5.4 and its applications, Geoscientific Model Development, 11, 1929–1969, https://doi.org/10.5194/gmd-11-1929-2018, publisher: Copernicus GmbH, 2018.

Lascaux, F., Richard, E., and Pinty, J.-P.: Numerical simulations of three different MAP IOPs and the associated microphysical processes, Quarterly Journal of the Royal Meteorological Society, 132, 1907–1926, https://doi.org/10.1256/qj.05.197, _eprint: https://rmets.onlinelibrary.wiley.com/doi/pdf/10.1256/qj.05.197, 2006.

Lasher-Trapp, S., Jo, E., Allen, L. R., Engelsen, B. N., and Trapp, R. J.: Entrainment in a Simulated Supercell Thunderstorm. Part I: The Evolution of Different Entrainment Mechanisms and Their Dilutive Effects, Journal of the Atmospheric Sciences, 78, 2725–2740, https://doi.org/10.1175/JAS-D-20-0223.1, publisher: American Meteorological Society Section: Journal of the Atmospheric Sciences, 2021.

LeBel, L. J. and Markowski, P. M.: An Analysis of the Impact of Vertical Wind Shear on Convection Initiation Using Large-Eddy Simulations: Importance of Wake Entrainment, Monthly Weather Review, 151, 1667–1688, https://doi.org/10.1175/MWR-D-22-0176.1, publisher: American Meteorological Society Section: Monthly Weather Review, 2023.

Maybee, B., Marsham, J. H., Klein, C. M., Parker, D. J., Barton, E. J., Taylor, C. M., Lewis, H., Sanchez, C., Jones, R. W., and Warner, J.: Wind Shear Effects in Convection–Permitting Models Influence MCS Rainfall and Forc-

https://doi.org/10.5194/egusphere-2026-323
Preprint. Discussion started: 29 January 2026

ing of Tropical Circulation, Geophysical Research Letters, 51, e2024GL110 119, https://doi.org/10.1029/2024GL110119, _eprint: https://onlinelibrary.wiley.com/doi/pdf/10.1029/2024GL110119, 2024.

Mazur, V. and Rust, W. D.: Lightning propagation and flash density in squall lines as determined with radar, Journal of Geophysical Research: Oceans, 88, 1495–1502, https://doi.org/10.1029/JC088iC02p01495, _eprint: https://agupubs.onlinelibrary.wiley.com/doi/pdf/10.1029/JC088iC02p01495, 1983.

Misumi, R., Divjak, M., Tanahashi, S., and Takeda, T.: A Numerical Study on the Formation of Organized Convective Storms: Part I. Formation Patterns of Long-Lasting Cells, Journal of the Meteorological Society of Japan. Ser. II, 72, 235–253, https://doi.org/10.2151/jmsj1965.72.2_235, 1994.

Mulholland, J. P., Peters, J. M., and Morrison, H.: How Does Vertical Wind Shear Influence Entrainment in Squall Lines?, Journal of the Atmospheric Sciences, 78, 1931–1946, https://doi.org/10.1175/JAS-D-20-0299.1, publisher: American Meteorological Society Section: Journal of the Atmospheric Sciences, 2021.

Peleg, N., Koukoula, M., and Marra, F.: A 2°C warming can double the frequency of extreme summer downpours in the Alps, npj Climate and Atmospheric Science, 8, 216, https://doi.org/10.1038/s41612-025-01081-1, publisher: Nature Publishing Group, 2025.

Peters, J., Hannah, W., and Morrison, H.: The Influence of Vertical Wind Shear on Moist Thermals, Journal of the Atmospheric Sciences, 76, https://doi.org/10.1175/JAS-D-18-0296.1, 2019.

Peters, J. M., Nowotarski, C. J., and Mullendore, G. L.: Are Supercells Resistant to Entrainment because of Their Rotation?, Journal of the Atmospheric Sciences, 77, 1475–1495, https://doi.org/10.1175/JAS-D-19-0316.1, publisher: American Meteorological Society Section: Journal of the Atmospheric Sciences, 2020.

Peters, J. M., Morrison, H., Nelson, T. C., Marquis, J. N., Mulholland, J. P., and Nowotarski, C. J.: The Influence of Shear on Deep Convection Initiation. Part I: Theory, Journal of the Atmospheric Sciences, 79, 1669–1690, https://doi.org/10.1175/JAS-D-21-0145.1, publisher: American Meteorological Society Section: Journal of the Atmospheric Sciences, 2022.

Pinty, J.-P. and Jabouille, P.: A mixed-phase cloud parameterization for use in mesoscale non-hydrostatic model: Simulations of a squall line and of orographic precipitations., in: Conference on Cloud Physics, 1998.

Pope, S. B.: Turbulent Flows, Cambridge University Press, 2000.

Prein, A. F., Liu, C., Ikeda, K., Trier, S. B., Rasmussen, R. M., Holland, G. J., and Clark, M. P.: Increased rainfall volume from future convective storms in the US, Nature Climate Change, 7, 880–884, https://doi.org/10.1038/s41558-017-0007-7, publisher: Nature Publishing Group, 2017.

Richards, F. and Arkin, P.: On the Relationship between Satellite-Observed Cloud Cover and Precipitation, Monthly Weather Review, 109, 1081–1093, https://doi.org/10.1175/1520-0493(1981)109<1081:OTRBSO>2.0.CO;2, publisher: American Meteorological Society Section: Monthly Weather Review, 1981.

Rio, C., Hourdin, F., Grandpeix, J.-Y., and Lafore, J.-P.: Shifting the diurnal cycle of parameterized deep convection over land, Geophysical Research Letters, 36, https://doi.org/10.1029/2008GL036779, _eprint: https://onlinelibrary.wiley.com/doi/pdf/10.1029/2008GL036779, 2009.

Rochetin, N., Hohenegger, C., Touzé-Peiffer, L., and Villefranque, N.: A Physically Based Definition of Convectively Generated Density Currents: Detection and Characterization in Convection-Permitting Simulations, Journal of Advances in Modeling Earth Systems, 13, e2020MS002 402, https://doi.org/10.1029/2020MS002402, _eprint: https://onlinelibrary.wiley.com/doi/pdf/10.1029/2020MS002402, 2021.

https://doi.org/10.5194/egusphere-2026-323
Preprint. Discussion started: 29 January 2026

Rooney, G. G., Stirling, A. J., Stratton, R. A., and Whitall, M.: C-POOL: A scheme for modelling convective cold pools in the Met Office Unified Model, Quarterly Journal of the Royal Meteorological Society, 148, 962–980, https://doi.org/10.1002/qj.4241, _eprint: https://rmets.onlinelibrary.wiley.com/doi/pdf/10.1002/qj.4241, 2022.

Rotunno, R. and Klemp, J. B.: The Influence of the Shear-Induced Pressure Gradient on Thunderstorm Motion, Monthly Weather Review, 110, 136–151, https://doi.org/10.1175/1520-0493(1982)110<0136:TIOTSI>2.0.CO;2, publisher: American Meteorological Society Section: Monthly Weather Review, 1982.

Siebesma, A. P., Bretherton, C. S., Brown, A., Chlond, A., Cuxart, J., Duynkerke, P. G., Jiang, H., Khairoutdinov, M., Lewellen, D., Moeng, C.-H., Sanchez, E., Stevens, B., and Stevens, D. E.: A Large Eddy Simulation Intercomparison Study of Shallow Cumulus Convection, Journal of the Atmospheric Sciences, 60, 1201–1219, https://doi.org/10.1175/1520-0469(2003)60<1201:ALESIS>2.0.CO;2, publisher: American Meteorological Society Section: Journal of the Atmospheric Sciences, 2003.

Strauss, C., Ricard, D., Lac, C., and Verrelle, A.: Evaluation of turbulence parametrizations in convective clouds and their environment based on a large-eddy simulation, Quarterly Journal of the Royal Meteorological Society, 145, 3195–3217, https://doi.org/10.1002/qj.3614, _eprint: https://onlinelibrary.wiley.com/doi/pdf/10.1002/qj.3614, 2019.

Takahashi, H. and Luo, Z.: Where is the level of neutral buoyancy for deep convection?, Geophysical Research Letters, 39, https://doi.org/10.1029/2012GL052638, _eprint: https://onlinelibrary.wiley.com/doi/pdf/10.1029/2012GL052638, 2012.

Thompson, R. L., Mead, C. M., and Edwards, R.: Effective Storm-Relative Helicity and Bulk Shear in Supercell Thunderstorm Environments, Weather and Forecasting, 22, 102–115, https://doi.org/10.1175/WAF969.1, publisher: American Meteorological Society Section: Weather and Forecasting, 2007.

Tippett, M. K., Allen, J. T., Gensini, V. A., and Brooks, H. E.: Climate and Hazardous Convective Weather, Current Climate Change Reports, 1, 60–73, https://doi.org/10.1007/s40641-015-0006-6, 2015.

Tobin, I., Bony, S., and Roca, R.: Observational Evidence for Relationships between the Degree of Aggregation of Deep Convection, Water Vapor, Surface Fluxes, and Radiation, Journal of Climate, 25, 6885–6904, https://doi.org/10.1175/JCLI-D-11-00258.1, publisher: American Meteorological Society Section: Journal of Climate, 2012.

Verrelle, A., Ricard, D., and Lac, C.: Sensitivity of high-resolution idealized simulations of thunderstorms to horizontal resolution and turbulence parametrization, Quarterly Journal of the Royal Meteorological Society, 141, 433–448, https://doi.org/10.1002/qj.2363, _eprint: https://onlinelibrary.wiley.com/doi/pdf/10.1002/qj.2363, 2015.

Weisman, M. L. and Klemp, J. B.: The Dependence of Numerically Simulated Convective Storms on Vertical Wind Shear and Buoyancy, Monthly Weather Review, 110, 504–520, https://doi.org/10.1175/1520-0493(1982)110<0504:TDONSC>2.0.CO;2, publisher: American Meteorological Society Section: Monthly Weather Review, 1982.

Weisman, M. L. and Klemp, J. B.: The Structure and Classification of Numerically Simulated Convective Stormsin Directionally Varying Wind Shears, Monthly Weather Review, 112, 2479–2498, https://doi.org/10.1175/1520-0493(1984)112<2479:TSACON>2.0.CO;2, publisher: American Meteorological Society Section: Monthly Weather Review, 1984.

White, B. A., Buchanan, A. M., Birch, C. E., Stier, P., and Pearson, K. J.: Quantifying the Effects of Horizontal Grid Length and Parameterized Convection on the Degree of Convective Organization Using a Metric of the Potential for Convective Interaction, Journal of the Atmospheric Sciences, 75, 425–450, https://doi.org/10.1175/JAS-D-16-0307.1, publisher: American Meteorological Society Section: Journal of the Atmospheric Sciences, 2018.